Cancer & Metabolism

RESEARCH

Open Access

The polyunsaturated fatty acid docosahexaenoic affects mitochondrial function in prostate cancer cells

Guilherme Henrique Tamarindo[1,2], Caroline Fidalgo Ribeiro[3], Alana Della Torre Silva[4], Alex Castro[2], Ícaro Putinhon Caruso[5,6], Fátima Pereira Souza[5], Sebastião Roberto Taboga[4], Massimo Loda[3] and Rejane Maira Góes[4*]

Abstract

Background Prostate cancer (PCa) shows a rewired metabolism featuring increased fatty acid uptake and synthesis via *de novo* lipogenesis, both sharply related to mitochondrial physiology. The docosahexaenoic acid (DHA) is an omega-3 polyunsaturated fatty acid (PUFA) that exerts its antitumoral properties via different mechanisms, but its specific action on mitochondria in PCa is not clear. Therefore, we investigated whether the DHA modulates mitochondrial function in PCa cell lines.

Methods Here, we evaluated mitochondrial function of non-malignant PNT1A and the castration-resistant (CRPC) prostate 22Rv1 and PC3 cell lines in response to DHA incubation. For this purpose, we used Seahorse extracellular flux assay to assess mitochondria function, [^{14}C]-glucose to evaluate its oxidation as well as its contribution to fatty acid synthesis, ^{1}H-NMR for metabolite profile determination, MitoSOX for superoxide anion production, JC-1 for mitochondrial membrane polarization, mass spectrometry for determination of phosphatidylglycerol levels and composition, staining with MitoTracker dye to assess mitochondrial morphology under super-resolution in addition to Transmission Electron Microscopy, In-Cell ELISA for COX-I and SDH-A protein expression and flow cytometry (Annexin V and 7-AAD) for cell death estimation.

Results In all cell lines DHA decreased basal respiratory activity, ATP production, and the spare capacity in mitochondria. Also, the omega-3 induced mitochondrial hyperpolarization, ROS overproduction and changes in membrane phosphatidylglycerol composition. In PNT1A, DHA led to mitochondrial fragmentation and it increased glycolysis while in cancer cells it stimulated glucose oxidation, but decreased *de novo* lipogenesis specifically in 22Rv1, indicating a metabolic shift. In all cell lines, DHA modulated several metabolites related to energy metabolism and it was incorporated in phosphatidylglycerol, a precursor of cardiolipin, increasing the unsaturation index in the mitochondrial membrane. Accordingly, DHA triggered cell death mainly in PNT1A and 22Rv1.

Conclusion In conclusion, mitochondrial metabolism is significantly affected by the PUFA supplementation to the point that cells are not able to proliferate or survive under DHA-enriched condition. Moreover, combination of DHA supplementation with inhibition of metabolism-related pathways, such as *de novo* lipogenesis, may be synergistic in castration-resistant prostate cancer.

*Correspondence:
Rejane Maira Góes
rejane.goes@unesp.br
Full list of author information is available at the end of the article

Keywords Prostate cancer cells, Omega-3 polyunsaturated fatty acids, Docosahexaenoic acid, Mitochondria, Lipid metabolism

Introduction

Prostate cancer (PCa) is among the main cause of death in men worldwide [1]. Most therapeutic strategies target the androgen receptor (AR) [2] which may select cells that are non-responsive to hormone ablation, leading to the castration-resistant prostate cancer (CRPC) that can ultimately result in lethality [3, 4]. This may occur due to several mechanisms, including alterations in AR levels by gene amplification and alternative splicing resulting in the AR-V7, which is constitutively active [5, 6].

Metabolic reprogramming is one of the hallmarks of cancer [7, 8]. Normal prostate cells mostly rely on glycolysis due to inhibition of tricarboxylic acid cycle (TCA) by androgens and high zinc concentration, leading to decreased mitochondrial activity [9, 10]. However, along PCa progression there is a shift towards lipid metabolism whereby cells rely on *de novo* lipogenesis (DNL) by remarkably increasing fatty acid synthase (FASN) expression while normal prostate cells display low levels of this enzyme [11–13]. Indeed, FASN co-localizes with both AR and AR-V7 in CRPC [14] and its genetic ablation or pharmacological inhibition leads to tumor growth suppression [15]. This indicates that lipid metabolism is crucial for PCa, in particular CRPC. Therefore, this scenario has driven efforts towards new therapeutic strategies targeting cell metabolism [16, 17].

Lipid metabolism is closely associated with mitochondrial function either for synthesis or oxidation. In PCa, exogenous fatty acids have been reported to exert distinct effect depending on their unsaturation status [18–21]. Saturated fatty acids drive PCa initiation and progression in part by enhancing the MYC program [20] while polyunsaturated fatty acids (PUFAs) may decrease cell and tumor growth [21] due to several mechanism, such as resolution of inflammation [22], modulation of metabolic pathways [23] and apoptosis induction [24]. We have previously reported that docosahexaenoic acid (DHA), a PUFA from the omega-3 class, delayed PCa progression in TRAMP mice [21] and, in CRPC cells, it accumulated into lipid droplets, induced oxidative stress and deregulated metabolism-related genes [23]. In addition, DHA led to structural mitochondrial alterations, mainly cristae misfolding, as well as mitophagy [23]. DHA effects on mitochondria has also been reported in other studies on PCa and linked to apoptosis, due to ROS overproduction [24], Bcl-2/caspase axis [25] and organelle perturbation [26]. Also, in PNT1A prostate cells the omega-3 was shown to impair the mitochondrial bioenergetic reserve capacity hence the cell ability to respond to additional insults [27].

This evidence on DHA property in affecting mitochondria is of particular interest given that PCa cells, androgen-responsive and androgen-independent, have increased mitochondrial mass [28, 29], pleomorphism [30] and overexpression of several genes related to biogenesis, bioenergetics and apoptosis [31] compared to normal cells (PrEC). In mitochondria, metabolic rewiring includes the increase in fatty acid beta-oxidation for energy supply and cell survival [32], a shift of their metabolism towards an oxidative phenotype [33], enhanced ATP production [34], but also the use of catabolic intermediates for DNL required for membrane synthesis and cell cycle progression [35]. In addition, mitochondria seem to be involved in AR signaling which is imported into mitochondria [36] where it regulates the organelle dynamics [37] and the expression of electron transport chain (ETC) complexes subunits [36]. Interestingly, enzalutamide-resistant PCa cells switch their metabolism from glycolysis to oxidative phosphorylation (OXPHOS) which was also observed in circulating tumor cells in patients that became resistant to such drug as well [38]. Therefore, several mitochondrial alterations are involved in PCa progression which could be used as a therapeutic strategy, especially in CRPC.

Among others omega-3, such as eicosapentaenoic acid (EPA) and α-linoleic acid (ALA), DHA is the one with the highest effectiveness in decreasing tumor cell viability and inducing apoptosis [39]. DHA has a low cost production and minimal side effects after its intake [40], being easily obtained from diet-enriched cold water marine fish with many benefits in health [41, 42]. Therefore, in the present study we evaluated whether DHA modulates mitochondrial physiology and metabolism of non-malignant and CRPC cells.

Material and methods

Cell culture and incubations

Prostate epithelial human cell lines PNT1A (#95012614 – Health Protection Agency, England, UK), 22Rv1 (#CRL-2505 – American Type Culture Collection, USA) and PC3 (#CRL1435 – American Type Culture Collection, USA) were cultured in RPMI 1640 medium (#R6504 – Sigma-Aldrich, USA; #11835030 – ThermoFischer Scientific, USA) supplemented with 10% fetal bovine serum (FBS) (#S0011—Vitrocell, Campinas, São Paulo, Brazil), 1% of penicillin, streptomycin, and amphotericin B (#15240062

– Life Technologies, UK) and kept in 5% of CO_2 at 37°C. For cell maintenance, the medium was replaced every 2–3 days and subculture done when confluence reached 80–90%. For experiments, cells were seeded at the desired density and attachment was allowed for 24 h.

Cells were incubated with DHA (#D2534—Sigma-Aldrich, USA) at 100 µM for 48 h, freshly prepared in the culture medium from 20 mM stock solution in anhydrous ethanol (vehicle). Concentration and time of incubation were chosen based on our previous study showing reduction of cell proliferation [23]. To ensure that the observed effects were mainly due to DHA, control assays were incubated with the same vehicle volume and used reagents from same brand and condition.

Seahorse XF Cell Mito Stress Test assay

Two 100 mm dishes were seeded with 2×10^6 cells each and incubated with DHA or vehicle. After 24 h of incubation, cells were collected with trypsin–EDTA 0.25%, counted, and reseeded at 2×10^4 density in Seahorse XF^{96} V3 PS Cell Culture Microplates (#101085–004, Agilent Technologies Inc, USA) with the same medium to avoid changes in the DHA concentration. Then, the Seahorse XF Cell Mito Stress Test assay (#103015–100, Agilent Technologies Inc, USA) was performed according to the manufactures' instructions. Briefly, Oligomycin (1 µM), FCCP (2 µM for PNT1A and 22Rv1; 0.5 µM for PC3) and Rotenone/Antimycin A (0.5 µM) were loaded at the cartridge ports. FCCP concentration and cell density per well were determined by prior titration experiments. Medium was removed from the microplate with the cells and replaced with warm and freshly prepared Seahorse XF Base Medium (#103681–100, Agilent Technologies Inc, USA), containing 1 mM pyruvate, 2 mM glutamine and 10 mM glucose (pH 7.4). Microplate coupled to the cartridge was placed at 37°C in non-CO_2 incubator for 45 min, followed by the determination of oxygen consumption (OCR) and Extracellular Acidification rates (ECAR) with Seahorse XFe96 Analyzer (Agilent Technologies Inc, USA). At the end of readings, cells in each well were lysed with RIPA buffer and total protein O.D. determined by BCA assay for normalization. Calculations were done by Wave software (v.2.6.3, Agilent) as follows: Basal Mitochondrial Respiration = (Late rate measurement before first injection) – (Non-mitochondrial respiration rate); Maximal Mitochondrial Respiration = (Maximum rate measurement after FCCP injection) – (Non-mitochondrial respiration rate); Proton Leak = (Minimum rate measurement after Oligomycin injection) – (Non-mitochondrial respiration); ATP-linked Production = (Late rate measurement before Oligomycin injection) – (Minimum rate measurement after Oligomycin injection); Spare Capacity = (Maximal Mitochondrial Respiration)—(Basal Mitochondrial Respiration); Non-mitochondrial respiration rate = Minimum rate measurement after Rotenone/ Antimycin A injection. Glycolytic Capacity was determined as ECAR rate upon Oligomycin injection. For statistical purpose, two independent experiments were performed with at least 10 replicates each ($n=20$). Values were shown as mean of $pmolO_2$/minute/ protein for OCR or mpH/minute/protein for ECAR plus SEM.

ATP levels

3×10^4 cells per well were seeded on white clear bottom microplates and at the end of the experiment, 100 µL of CellTiter-Glo® 2.0 Assay (#G9241, Promega, USA) at room temperature (RT) were added to each well and incubated for 10 min under shaking. Then, Relative Luminescence Units (RLU) was determined with SpectraMax iD5 microplate reader (Molecular Devices) and 25 µL of samples collected from each well to perform BCA assay for normalization to protein. Three independent experiments were performed with at least 3 replicates each ($n=9$). Values were shown as mean of fold-change and SEM.

[^{14}C]-Glucose oxidation and incorporation into lipids

Glucose complete oxidation was determined by [^{14}C]-CO_2 release after incubation with [^{14}C]-Glucose (ARC-0122D). Cells were seeded at 0.5×10^6 density in a 60 mm dish and incubated with DHA for 48 h in RPMI 1640 medium containing glucose at 2 g/L. Two hours prior to the end of the experiment, 0.5 µCi/µl of [^{14}C]-Glucose was added in the dish. At the end of incubation 100 µL of 70% perchloric acid were added to the dish and immediately closed with a trapped Whatman filter grade 3 circle saturated with 200 µL of phenethylamine. [^{14}C]-CO_2 capture was allowed for 2 h at RT under slow shaking and circles collected for quantification. Lipogenesis from glucose carbons were determined at same conditions, but for this assay [^{14}C]-Glucose was added to the dish at 1 µCi/well 24 h before the end of the experiment [14]. At the end of incubation, cells were harvested with trypsin–EDTA 0.25%, centrifuged at 300 g for 5 min at 4°C, washed with cold PBS, and pelleted down. Then, cells were lysed with cold extraction solution (2 mL methanol, 1 mL chloroform and 0.5 mL of dH_2O) in glass tubes and incubated overnight at -20°C. Samples were centrifuged at 400 g for 10 min at 4°C, and the supernatant was collected for lipophilic fraction extraction with cold chloroform (1 mL) and dH_2O (1 mL). Lipophilic phase was collected and dried at 50°C under nitrogen flux to avoid oxidation. Lyophilized samples were resuspended in 500 µL of cold Bligh & Dyer solution (2:1 volume of methanol:chloroform). For both assays,

radioactivity was determined by liquid scintillation in vials containing 10 mL of UltraGold™ (#6013326 – PerkinElmer) and assessed with β-counter (Tri-carb 2910 TR Liquid Scintillation Counter, PerkinElmer). Counts per minute (CPM) were normalized to viable cells, assessed by automated counter Vi-Cell Blue XR (Beckman Coulter, USA) based on the trypan blue exclusion method. Values were shown as fold-change to control and SEM. At least three independent experiments were performed for statistical analysis ($n=6$).

^{1}H-NMR Metabolomics

For metabolomics analysis, 10^6 cells were seeded in culture flasks and allowed 48 h for expansion prior to DHA incubation. Briefly, cells were removed with 0.25% trypsin–EDTA, centrifuged at 2000 rpm for 5 min at 4°C, washed twice in cold PBS and pellet embedded in liquid nitrogen for quenching at least 10 min. Three consecutive and independent experiments were performed ($n=7$) and samples were stored at -80°C. For analysis, 4×10^6 cells were resuspended in 650 µL of filtered methanol 80%, 220 µL of filtered dH_2O and vortexed. Then, samples were sonicated to complete cell lysis, added 420 µL of chloroform, vortexed again, kept on ice for 10 min and centrifuged at 16,000 g for 20 min at 4°C. Hydrophilic phase was collected and dried in vacuum centrifuge for 4 h at 45°C. Then, it was resuspended in 600 µL of phosphate deuterated buffer (100 mM pH 7,4; 0,150 mM DSS). Each phase was transferred to 5 mm NMR tube and spectra were collected in Bruker Avance HD III spectrometer operating at 600 MHz. All measurements were performed at 298 K. The standard Bruker 1D pulse sequence NOESYPR1D was used with a mixing time of 300 ms. A total of 512 scans were collected with 16 dummy scans, and a spectral width of 20 ppm and 32 k data points were used. Relaxation delay was set to 2 s with 0.2 ms of gradient recovery. A line broadening of 1 Hz was applied to each free induction decay (FID) before Fourier transformation. Following, each spectrum was automatically phase corrected and referenced to the 3-(Trimethylsilyl)-1-propanesulfonic acid-d6 sodium salt (DSS-d6) at 0.0 ppm. To aid in metabolite identification, 2D ^{1}H-^{1}H Total Correlation Spectroscopy (TOCSY) experiments were performed using a DPSI sequence for mixing and pre-saturation for water suppression in selected samples. A mixing time of 80 ms was chosen, and spectra were collected using 32 scans with 2 k data points in the direct dimension and 256 data points in the indirect dimension. Relaxation delay was maintained at 2 s.

For data processing, noise and water signal regions were removed from raw data. Metabolites from NMR spectra were assigned using Chenomx Profiler software (NMR Suite v.10.1, Chenomx Inc; Edmonton, Canada) library which was also used to estimate their concentration (Table S1). Then, concentrations were submitted to MetaboAnalyst 5.0 tool [43] to calculate the principal component analysis (PCA; Fig. S1) as well as to generate the heatmap for each cell line after sum normalization and Pareto scaling. Features were scaled to a *z*-score and clustered by Euclidean distance and Ward method. To determine the statistically different metabolites a t-test ($p<0.05$) and false discovery rate (FDR) of 0.1 were applied. Metabolites statistically significant underwent verification using 2D ^{1}H-^{1}H TOCSY experiments (Fig.S2; S3) in the TopSpin software 4.0.7 (Bruker BioSpin GmbH, 2019). Only the statistically significant metabolites were plotted in the bar graphs and values shown as the mean of relative concentration to sum and SEM.

Phosphatidylglycerol quantification and lipid saturation profile

Cells were seeded at 10^6 density and, after DHA incubations, collected with trypsin–EDTA 0.25%, centrifuged at 300 g for 5 min at RT and pellets stored at -80°C. Samples were shipped out and processed by Lipometrix (Leuven, Belgium). Briefly, cells homogenized in water (volume equivalent to 20 µg of protein) were mixed with 800 µl 1 N HCl:CH_3OH 1:8 (v/v), 900 µl $CHCl_3$, 200 µg/ml of the antioxidant 2,6-di-tert-butyl-4-methylphenol (BHT; Sigma Aldrich) and 3 cl of SPLASH® LIPIDOMIX® Mass Spec Standard (#330707, Avanti Polar Lipids). After vortexing and centrifugation, the lower organic fraction was collected and evaporated using a Savant Speedvac spd111v (Thermo Fisher Scientific) at RT and the remaining lipid pellet used for analysis after reconstitution in absolute ethanol. Lipid species were analyzed by liquid chromatography electrospray ionization tandem mass spectrometry (LC-ESI/MS/MS) on a Nexera X2 UHPLC system (Shimadzu) coupled with hybrid triple quadrupole/linear ion trap mass spectrometer (6500 + QTRAP system; AB SCIEX). Chromatographic separation was performed on a XBridge amide column (150 mm × 4.6 mm, 3.5 µm; Waters) maintained at 35°C using mobile phase A [1 mM ammonium acetate in water-acetonitrile 5:95 (v/v)] and mobile phase B [1 mM ammonium acetate in water-acetonitrile 50:50 (v/v)]. Phosphatidylglycerol (PG) was measured in negative ion mode by fatty acyl fragment ions. Lipid quantification was performed by scheduled multiple reactions monitoring (MRM). Peak integration was determined with the MultiQuant™ software version 3.0.3. Signals were corrected for isotopic contributions (calculated with Python Molmass 2019.1.1), quantified based on internal standard signals and adheres to the guidelines of the Lipidomics Standards Initiative (LSI) (level 2 type quantification as

defined by the LSI). Three independent experiments were performed ($n=3$) for each condition and cell line.

Mitochondrial membrane potential and superoxide anion quantification

To determine the mitochondrial membrane polarization, we performed a ratiometric assay with JC-1 dye (#ab113850, Abcam, USA). Cells were seeded at 3×10^4 density per well in a black microplate with clear bottom and, at the end of the experiment, warmed JC-1 was added to reach 10 µM in the wells. After incubation for 20 min at 37°C, the dye was removed, and wells washed twice with 1X dilution buffer provided by the manufacturer. Relative Fluorescence Units (RFU) were assessed at 535/590 nm and 475/530 nm to quantify aggregated and monomeric forms, respectively. Mitochondrial membrane potential was determined by the ratio of aggregates RFU to monomers. FCCP at 100 µM was added 4 h prior to JC-1 in one well and used as a reference for mitochondrial membrane depolarization. Values were shown as mean and SEM.

Superoxide anion production was assessed by MitoSOX™ Red dye (#M36008, ThermoFischer). Cells were incubated at 3×10^4 density per well in a black microplate with clear bottom and, at the end of DHA incubation, the medium was replaced with 5 µM of the dye, followed by 20 min of incubation at 37°C. Then, wells were washed in warm PBS and RFU was assessed at 510/580 nm. At the end of readings, RIPA buffer was added to each well and protein content was determined by BCA assay for normalization. Values were shown as fold-change and SEM. For both assays described in this section, three independent experiments were performed ($n=7$ at least) and RFU was collected with SpectraMax iD5 microplate reader (Molecular Devices).

Mitochondria morphology

To assess mitochondria morphology and distribution, cells at 10^4 density/well were seeded in CELL^{view} slide (#543999 – Greiner Bio-one). Mitochondria and nuclei visualization was done after staining with MitoTracker Orange CMTMRos (#M7510 Molecular Probes, Invitrogen) at 50 nM and Hoechst 33342 at 1 µg/mL, respectively. After 15 min of incubation at 37°C and 5% CO_2, the staining solution was removed, and cells were fixed with 4% paraformaldehyde, washed twice in PBS and slide covered with mounting media. Mitochondria network was assessed at 554/576 nm with an inverted super-resolution microscope AiryScan LSM880 (Carl Zeiss AG, Germany) and DNA at 350/461 nm at 63× objective. Maximum projection image was adopted for analysis. Transmission Electron Microscopy was performed to confirm mitochondrial fragmentation. Briefly, 2×10^6 cells were seeded, pelleted and immersed in a fixation solution (2% paraformaldehyde, 2.5% glutaraldehyde and 0.25% $CaCl_2$ in 0.1 M cacodylate buffer – pH 7.4) for 2 h at RT. Pellets were post-fixed in 2% osmium tetroxide in 0.1 M cacodylate for 1 h at RT. Then, samples were immersed in 0.5 uranyl acetate for 1 h, dehydrated in acetone and embedded in araldite resin. Ultrathin sections were placed onto grid and stained with 2% alcoholic uranyl acetate and 2% lead citrate in 1 N sodium hydroxide for 10 min. Images were acquired using a JEOL 1400Plus microscope.

In-Cell ELISA

MitoBiogenesis™ In-Cell ELISA Kit (#ab140359, Abcam) was used to determine the mitochondrial-encoded and nuclei-encoded gene expression ratio. For this purpose, cells at 3×10^4 density per well were seeded in a black clear bottom microplate. Relative Fluorescence Units (RFU) of succinate dehydrogenase A (SDH-A) and subunit I of Complex IV (COX-I) were determined according to manufactures' instructions and normalized to Janus Green optical density measured at 595 nm to account for differences in cell density. Readings were collected with SpectraMax iD5 microplate reader (Molecular Devices). Three independent experiments were performed with at least 3 replicates each ($n=9$).

Annexin V assay

Cell death was assessed by flow cytometry using the BD Pharmingen™ Annexin V Apoptosis Detection Kit I (#559763, BD Biosciences). Briefly, cells were seeded at 10^6 density and, at the end of DHA incubation, collected with trypsin–EDTA 0.25%, centrifuged at 1500 RPM for 5 min at RT and stained according to the manufacturer's instructions. Cell populations were immediately gated as viable (Annexin V-/7-AAD-), early apoptosis (Annexin V+/7-AAD-), late apoptosis (Annexin V+/7-AAD+) and potentially necrosis (Annexin V-/7-AAD+). Data was acquired for 2×10^4 events with BD FACS Canto II using BD FACS Diva™ software and analyzed with Flowing 2.5.1 software. Values were shown as fold-change from two independent experiments and a representative flow cytometry chart was plotted for each tested condition with mean of events.

Statistical analysis

Statistical analyses were performed with GraphPad Prism® software (v.9.2.0). First, the distribution of samples was analyzed with Kolmogorov–Smirnov and Shapiro–Wilk normality tests. Parametric distributions were submitted to unpaired *t*-test and non-parametric distributions to Mann–Whitney. The significance level was set at 5% ($p<0.05$).

Results

DHA impairs mitochondrial function, ATP production and the spare capacity

We reported previously that DHA at same conditions adopted here led to a decrease in cell growth followed by deregulation of several metabolism-related genes [23]. It also induced alterations in mitochondria ultrastructure [23], but further alterations were not assessed. Therefore, in the present study we lean on several parameters to understand whether DHA affects mitochondria function. Firstly, we performed a Seahorse MitoStress test. Figure 1A-B and C-D show the OCR and ECAR representative profiles, respectively, after incubation with DHA or vehicle for each cell line. The omega-3 decreased the

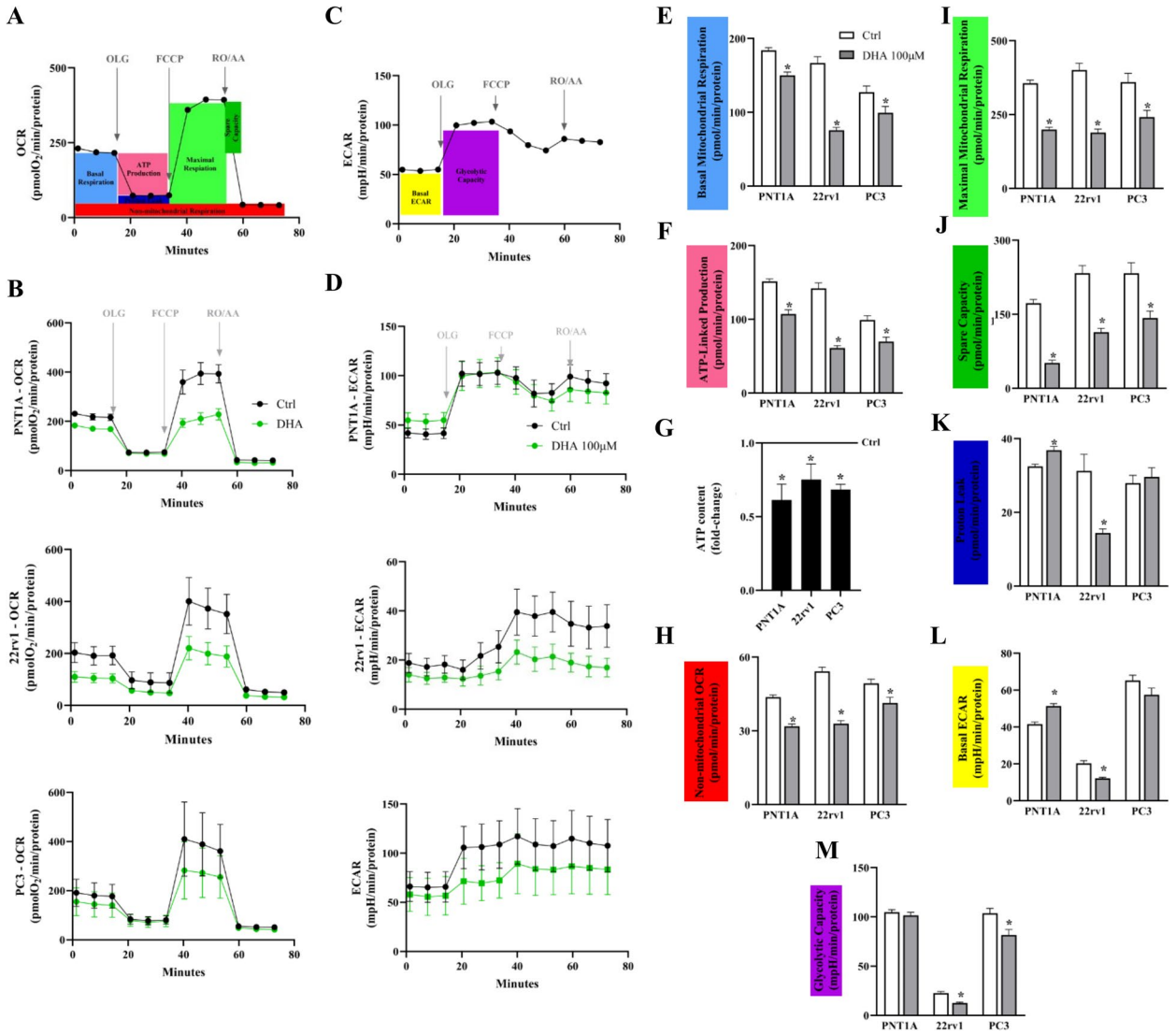

Fig. 1 DHA induces mitochondria dysfunction in PNT1A and castration-resistant prostate cells. **A** Example of Oxygen Consumption Rates (OCR) calculated for each respiratory parameter from Seahorse data and (**B**) their representative profiles for each cell line after normalization. **C** Example of Extracellular Acidification Rate (ECAR) calculated for each respiratory parameter from Seahorse data and (**D**) their representative profiles for each cell line after normalization. Black and green lines show control and DHA-treated cells, respectively. **E** Basal Mitochondrial Respiration without any inhibitors indicated mitochondria activity reduction. **F** OCR required for ATP-linked production and (**G**) ATP content, measured by mono-oxygenation of luciferin. **H** Non-mitochondrial respiration OCR. **I** Maximum Mitochondrial Respiration and (**J**) Spare capacity showed that DHA decreased the bioenergetic reserve. **K** Proton Leak. OCR values show mean and SEM of pmolO_2/minute/protein ($n = 20$, two independent experiments) while ATP content indicates fold-change relative to control ($n = 9$, three independent experiments). **L** Basal ECAR and (**M**) ECAR under oligomycin inhibition, suggesting glycolytic capacity. Values show mpH/minute/protein O.D. and SEM ($n = 20$, two independent experiments). Legend: Ctrl – vehicle incubation; DHA – docosahexaenoic acid; *—statistically different from control ($p < 0.05$) after unpaired *t*-test

basal mitochondrial respiration in all cell lines (Fig. 1E), with the strongest effect on 22Rv1 (54%). The OCR required for ATP-linked production also decreased in the same manner (Fig. 1F). The reduction in ATP levels was confirmed by specific assay (Fig. 1G) in all cell lines (39% in PNT1A, 25% in 22Rv1 and 32% in PC3). Non-mitochondrial oxygen consumption decreased upon DHA incubation (Fig. 1H). Then, we used mitochondrial stress test data to evaluate several respiratory parameters, such as maximal mitochondrial respiration and the organelle ability to respond to stress, also known as spare capacity. We observed that in all cell lines, DHA decreased both maximal mitochondrial respiration (Fig. 1I) and the spare capacity (Fig. 1J) which had the strongest effect in PNT1A (70%) compared to 22Rv1 (51%) and PC3 (30%). Mitochondrial dysfunction and ROS production are related to proton leak, which we confirmed to be increased in PNT1A but decreased in 22Rv1 while remaining unchanged in PC3 (Fig. 1K). Next, to understand whether cells rely on glycolysis, we analyzed the Basal ECAR (Fig. 1L) and estimated the glycolytic capacity (Fig. 1M) in addition to CO_2 production (Fig. 2A) and lipogenesis (Fig. 2B) from [^{14}C]-glucose carbons. In the absence of any perturbation, DHA increased around 23% the Basal ECAR in PNT1A and reduced it 40% in 22Rv1, but no change was observed in PC3. Upon inhibition of mitochondrial ATP synthesis (Fig. 1M), ECAR reduced only in tumor cells (40% 22Rv1 and 20% PC3), suggesting an impairment of glycolytic capacity. Given these alterations in ECAR, we looked at glucose metabolism, specifically to its oxidation and accumulation into lipids using [^{14}C]-Glucose. Complete glucose oxidation (Fig. 2A) increased in tumor cells at least 1.2-fold but remained unchanged in PNT1A. Lipogenesis from glucose (Fig. 2B) decreased in 22Rv1 while increased in PC3 and unchanged in PNT1A. Lactate intracellular

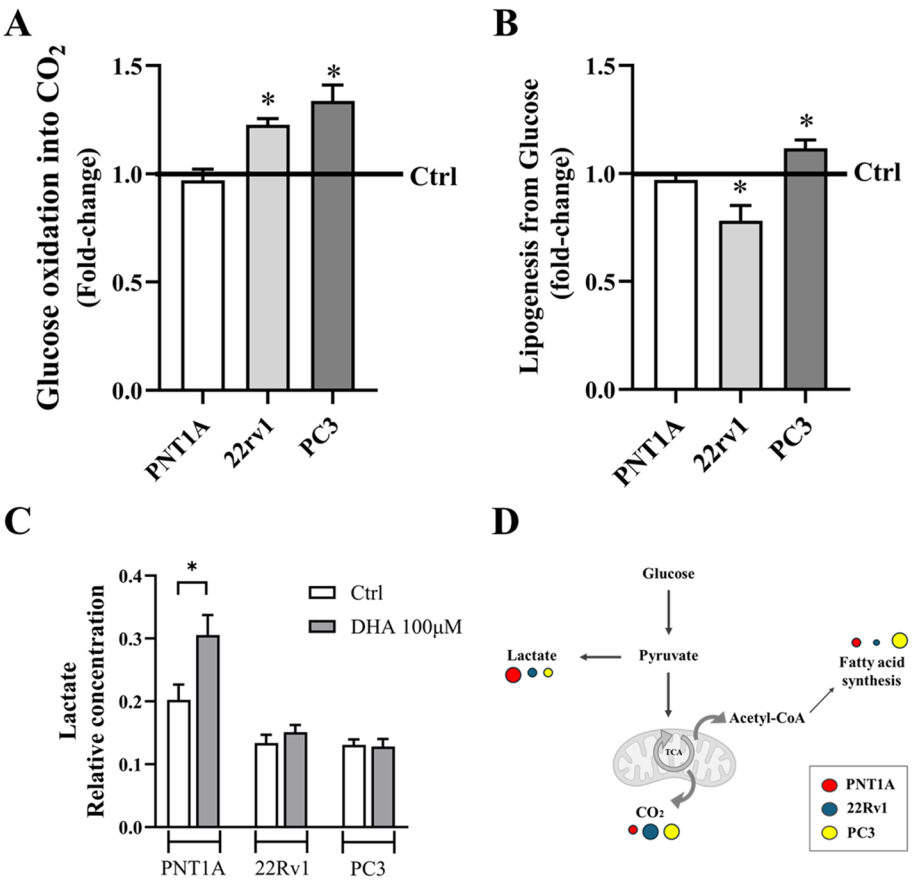

Fig. 2 DHA affects glucose metabolism. **A** [^{14}C]-CO_2 production from [^{14}C]-glucose oxidation is increased in castrated-resistant cells. [^{14}C] cells. **B** Lipogenesis from [^{14}C]-glucose carbons is decreased in 22Rv1, increased in PC3 and unchanged in PNT1A cells.[^{14}C]-CO_2 [^{14}C]ant cells. Values shown as mean of fold-change of CPM/viable cells related to control (vehicle) and SEM. **C** Lactate intracellular levels from ^{1}H-NMR experiment. Values were shown as mean of relative concentration to sum and SEM. **D** Proposed rewire of glucose metabolism. Large circles mean increase while smaller circles decrease in PNT1A (red), 22Rv1 (blue) and PC3 (yellow). Legend: Ctrl – vehicle incubation; DHA – docosahexaenoic acid; *—statistically different from control ($p < 0.05$) after unpaired *t*-test

levels increased only in PNT1A cells (Fig. 2C). Metabolomics data by ^{1}H-NMR showed that DHA modulated the metabolite profile (Fig. 3). In PNT1A (Fig. 3A-B), the omega-3 increased leucine, s*n*-glycero-3-phosphocholine, choline, glycerol and isoleucine while decreased myo-inositol, glutamate, o-phosphocholine, aspartate and creatine. In 22Rv1 (Fig. 3C-D), DHA raised leucine, glutathione, sn-glycero-3-phosphocholine, choline, isoleucine and UDP-N-Acetylglucosamine while reduced o-acetylcholine and aspartate. Lastly, in PC3 (Fig. 3E-F) DHA increased creatine phosphate and NAD+while decreased only myo-inositol.

DHA induces ROS production, mitochondrial membrane hyperpolarization and changes in PG unsaturation status

To better understand such changes behind the metabolic effect, we looked at mitochondrial membrane polarization using JC-1 dye (Fig. 4A), as it is directly associated with ROS production, mitochondrial function, and apoptosis. We found that DHA triggered mitochondrial membrane hyperpolarization in all cell lines (PNT1A 27%; 22Rv1 92%; PC3 23%). The omega-3 increased ROS production at least 1.5-fold compared to vehicle in all cell lines (Fig. 4B), supporting the mitochondrial dysfunction. As to membrane composition, we assessed the total levels and composition of the main phospholipid found in mitochondria and precursor of cardiolipin (CL), phosphatidylglycerol (PG) by mass spectrometry (Fig. 4C-F). Its absolute levels decreased 65% in PNT1A (Fig. 4C) followed by an increase in the unsaturation level in PG fraction, as shown in the bar graphs in Fig. 4D. Among the fatty acids in PG, mostly those with 20 and 22 carbons increased (Fig. 4D). Regarding tumor cells, PG absolute levels increased at least 40% (Fig. 4C) as well as the level of saturated and monounsaturated fatty acids in PG fraction (Fig. 4E-F, bar graphs). In all cell lines, 22:6 fatty acids concentration increased, indicating DHA incorporation into PG (Fig. 4D-F, heatmaps). Also, there was an increase of 20:5 fatty acids concentration (EPA) in PG (Fig. 4D-F, heatmaps), indicating its conversion from 22:6 fatty acid.

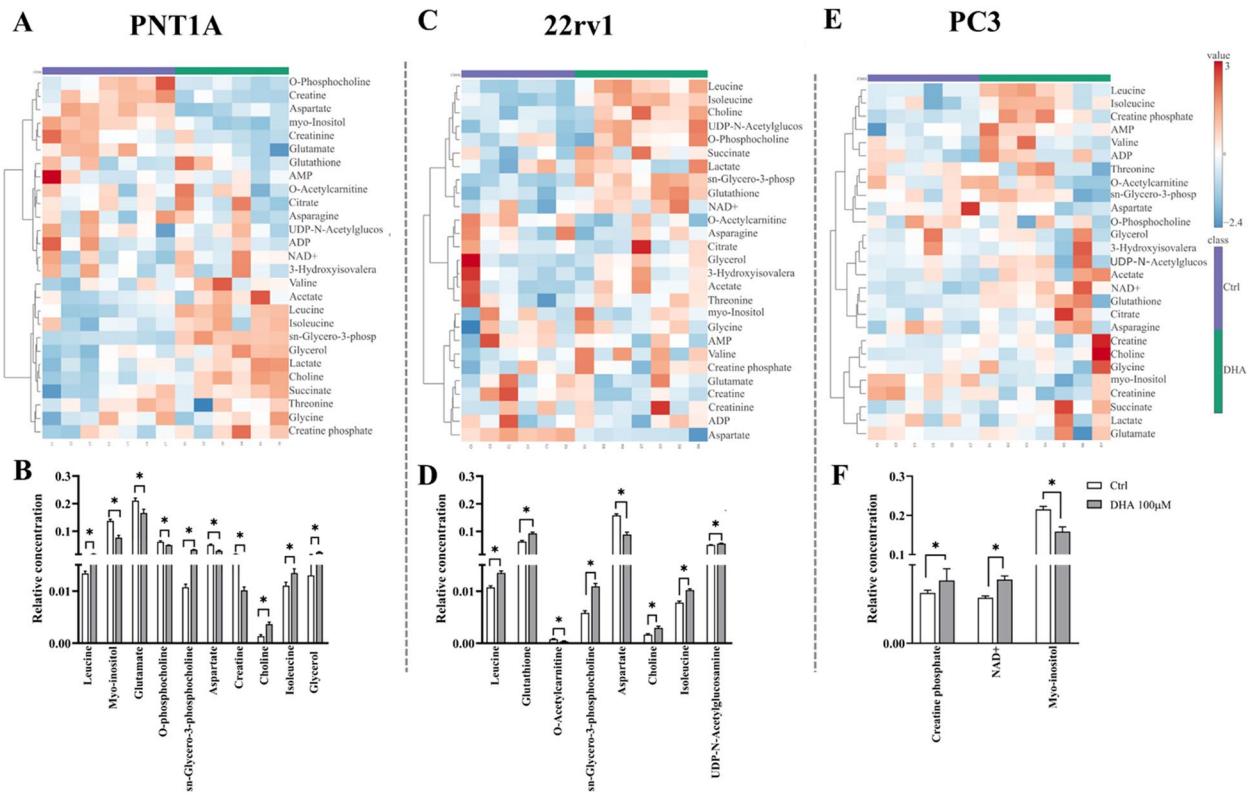

Fig. 3 DHA changed the metabolites profile. Heatmap and relative quantification of assigned metabolites for (**A**–**B**) PNT1A, (**C**–**D**) 22Rv1 and (**E**–**F**) PC3 identified by ^{1}H-NMR after incubation with DHA at 100 μM for 48 h. Heatmaps were generated using *z*-score and features were clustered. Red squares mean increased concentration while blue decreased. Values in the bar graphs show the mean of relative concentration to sum and SEM ($n = 6$/group at least, three independent experiments) for statistically significant metabolites. Legend: NAD+—nicotinamide adenine dinucleotide; Ctrl – vehicle incubation; DHA – docosahexaenoic acid; *—statistically different from control ($p < 0.05$ and FDR = 0.1) after unpaired *t*-test

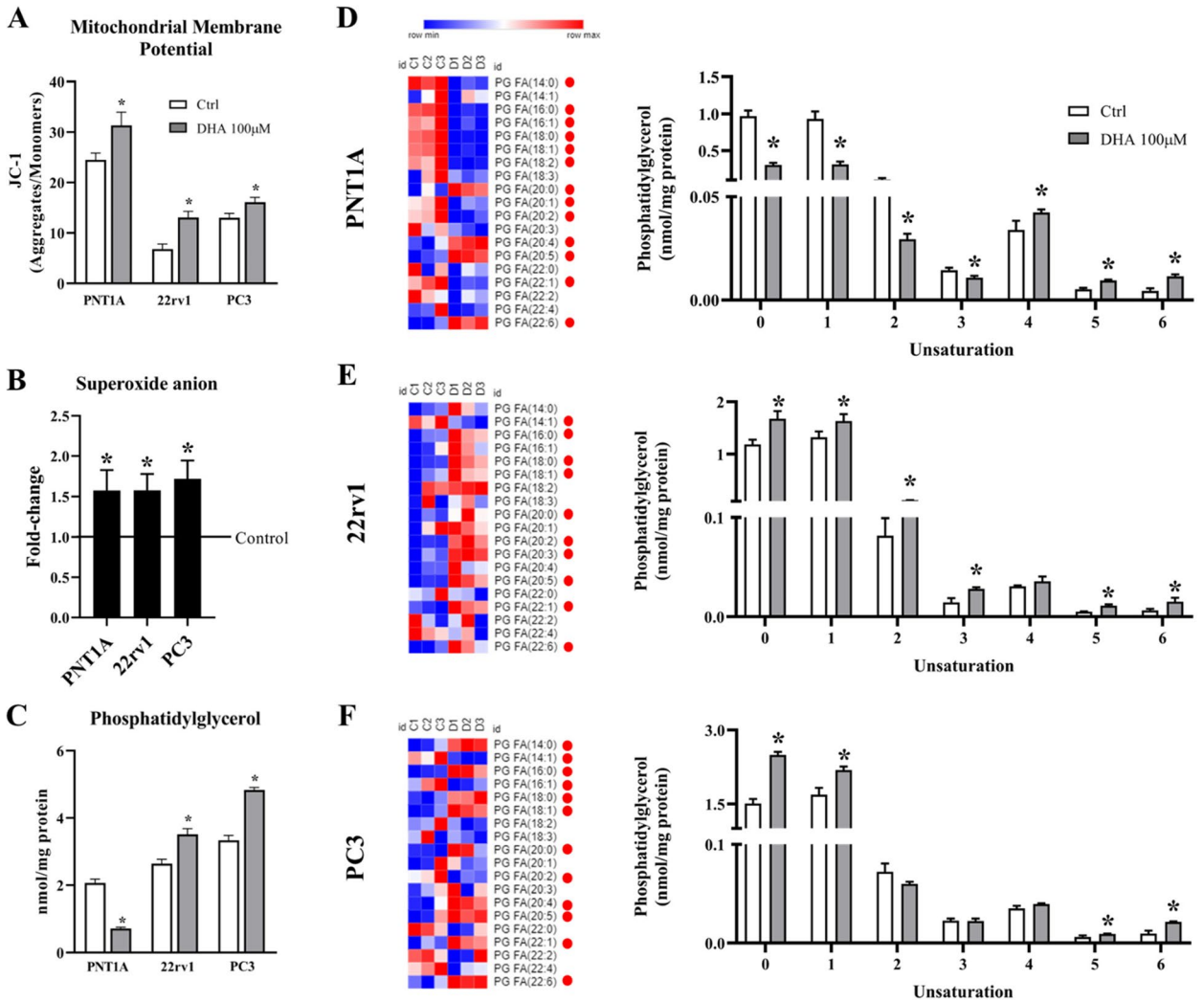

Fig. 4 DHA leads to mitochondria hyperpolarization, $O_2^{\bullet-}$ overproduction and changes in phosphatidylglycerol composition. **A** Increase in mitochondria membrane potential after DHA incubation, assessed with JC-1 dye. Values show the mean of J-aggregates to monomers ratio and SEM ($n = 9$). **B** $O_2^{\bullet-}$ overproduction determined by MitoSOX Red. Values show the mean of fold-change relative to control and SEM ($n = 9$). **C** Phosphatidylglycerol concentrations in each cell line after DHA or vehicle incubation. Values show the mean of nmol/mg of protein and SEM ($n = 3$). **D**-**F** Heat maps on the left display the most significant phosphatidylglycerol fatty acid composition determined by mass spectrometry. Red squares in each row mean increase and blue decrease in concentration (nmol/mg protein) scaled to *z*-score. Red dots showed statistically different compared to the control. Graphs on the right side indicate the sum by unsaturation in among all PG detected. Values show mean of nmol/mg protein and SEM ($n = 3$). Three independent experiments were performed for statistical analysis. Legend: Ctrl – vehicle incubation; DHA – docosahexaenoic acid; FA – fatty acid; PG – phosphatidylglycerol; *—statistically different from control ($p < 0.05$) after unpaired *t*-test

DHA stimulates mitochondria fragmentation in non-malignant cells

Considering mitochondrial activity assumes distinct morphology depending on its metabolic activity, we evaluated whether DHA impacts the mitochondrial network and ultrastructure. The omega-3 induced mitochondria fragmentation in PNT1A, evidenced by round mitochondria under super-resolution microscopy and the ultrastructure assessed by TEM (Fig. 5A-B). This was not observed in tumor cells since their mitochondria were more elongated and had same morphology than control incubation (Fig. 5A-B). However, both non-malignant and PCa cells showed cristae damage and misfolding in the mitochondria ultrastructure (Fig. 5B).

To determine whether such fragmentation affected the balance between nuclei- and mitochondria-encoded proteins expression, usually performed to evaluate biogenesis, we assessed SDH-A and COX-I by In-Cell ELISA in addition to their ratio. DHA induced SDH-A (Fig. 5C) and COX-I expression (Fig. 5D) in

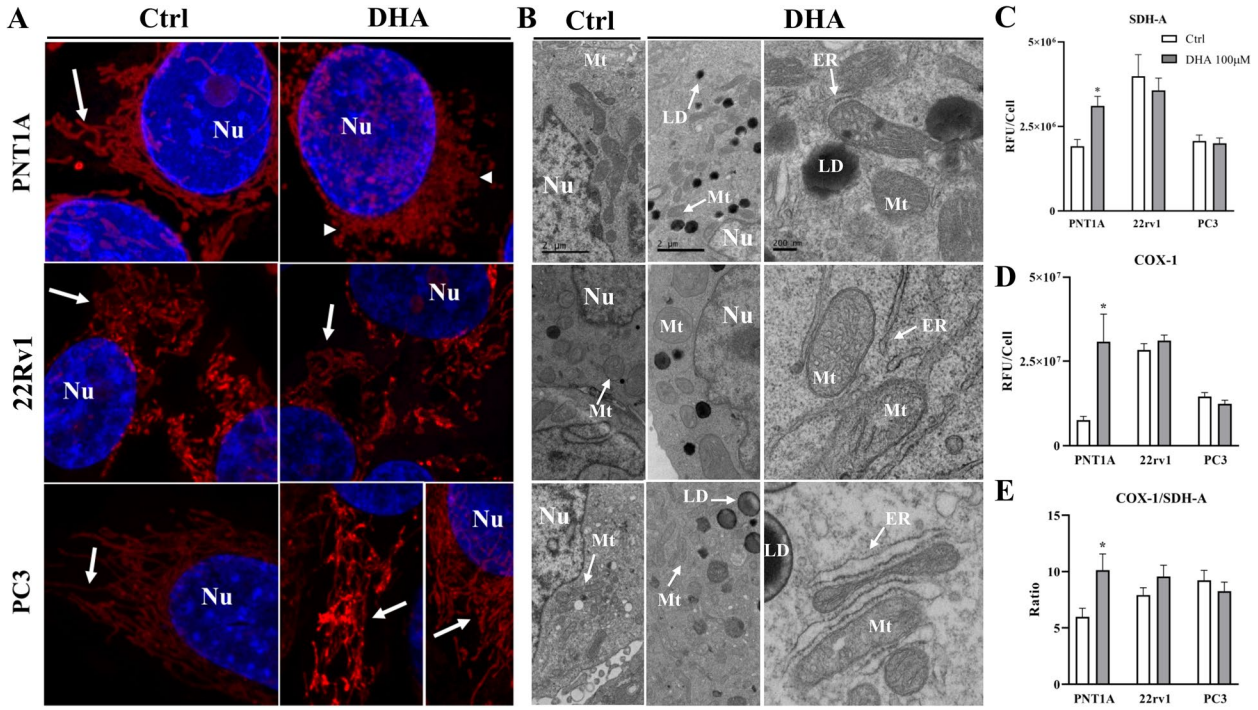

Fig. 5 DHA induces mitochondria fragmentation in PNT1A and organelle damage in CRPC cells. **A** Mitochondria network in red and nuclei in blue (Nu) evidenced by MitoTracker Orange CMTMRos dye and Hoechst 33342, respectively. Arrows point to elongated mitochondria, whereas arrowhead to the fragmented. Images were captured at 400× magnification. **B** Ultrastructure of prostate cells by TEM. Images validate mitochondrial fragmentation in the first two columns (bar 2 μm) and damage in the third (bar 200 nm). **C** Expression of Succinate dehydrogenase A (SDH-A), a nuclei-encoded protein, (**D**) Subunit I of Complex IV (COX-I), a mitochondria-encoded, and (**E**) COX-I to SDH-A ratio. Values show the mean of Relative Fluorescence Units (RFU) per cell and SEM. Three independent experiments were performed for statistical analysis. Legend: Ctrl – vehicle incubation; DHA – docosahexaenoic acid; Nu – nucleus; LD – lipid droplet; Mt – mitochondria; ER – endoplasmic reticulum; * – statistically different from control ($p < 0.05$) after unpaired *t*-test

PNT1A. In addition, there was an increase in COX-1 to SDH-A ratio (Fig. 5E) in this cell line, indicating an imbalance in their expression supporting mitochondrial impairment.

DHA induces cell death in AR-positive cells

We showed here mitochondria membrane hyperpolarization (Fig. 4A) and increase in unsaturation status in PG in the mitochondrial membrane, both strictly related cell death and ROS overproduction. Therefore, we estimated early and late apoptosis in addition to potential necrosis by flow cytometry using Annexin V and 7-AAD staining (Fig. 6). Regarding PNT1A cells, we found that, on average DHA induced 2.2-fold more late apoptosis events than vehicle (Fig. 6A-C). For tumor cells, apoptosis was observed only in 22Rv1, being 1.6- more early events and 1.5-fold the late apoptosis (Fig. 6D-F). However, cell death seemed not to be triggered by DHA on PC3 (Fig. 6G-I).

Discussion

The reliance on mitochondrial pathways varies with PCa progression and its vulnerabilities have been explored as a therapeutic alternative in the disease [44]. However, the role of fatty acids, mainly DHA remained unclear. We reported previously that prostate cells are not able to maintain proliferation or survival in DHA-enriched condition, regardless of being non-malignant or malignant [23], but the underlying mechanisms were not fully elucidated. Here we described that DHA induces mitochondrial dysfunction due to OXPHOS impairment in the three cell lines investigated, as indicated by the decrease in the basal mitochondrial respiration, in the spare capacity, ATP production and ROS overproduction. However, it seemed to rewire glucose utilization by stimulating glycolysis in non-malignant cells, evidence supported by the raise in lactate levels. Despite not previously reported for PNT1A, the glycolytic phenotype is associated with mitochondria fragmentation [45], as we showed here. In the CRPC

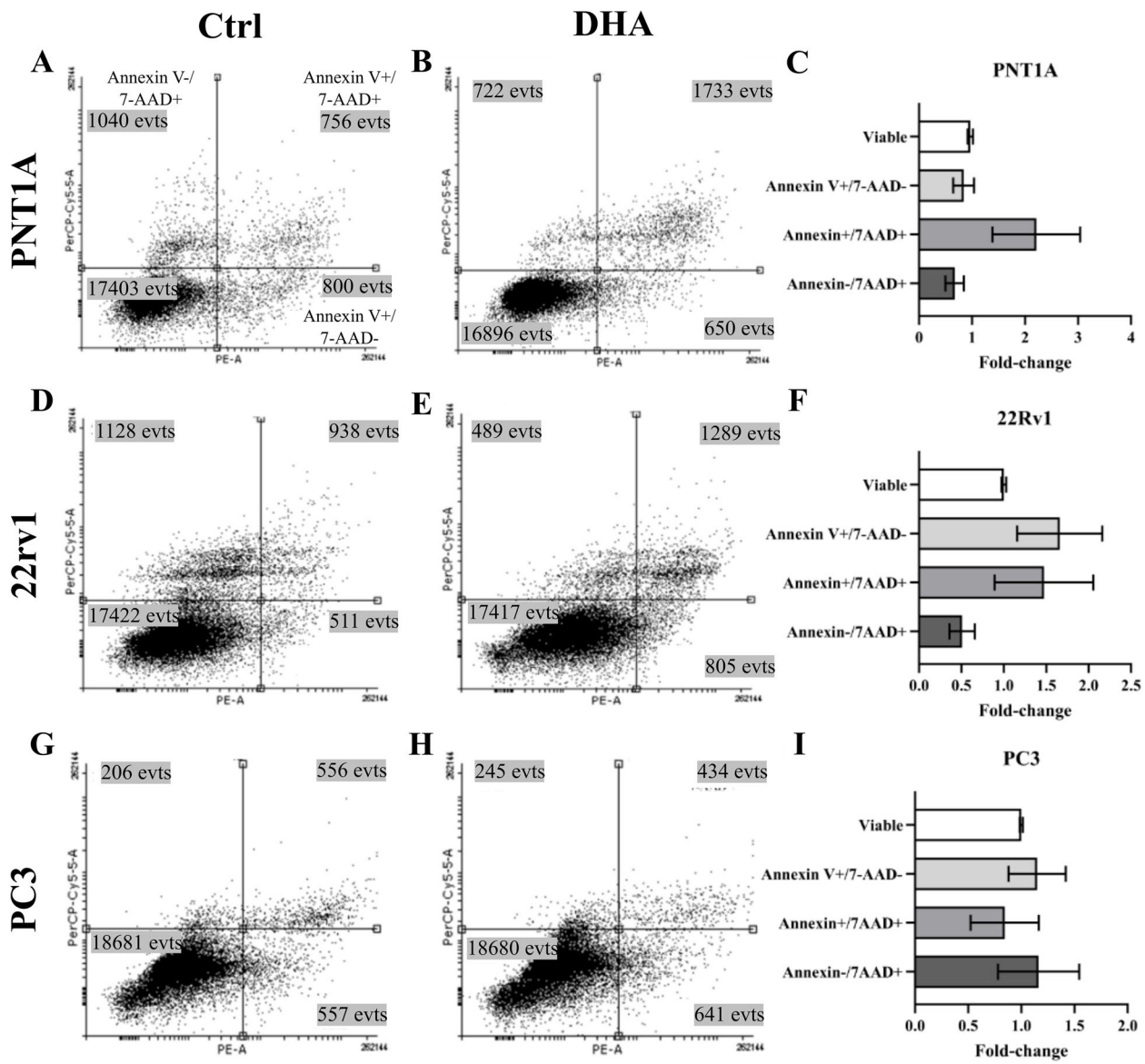

Fig. 6 DHA triggers apoptosis in PNT1A and 22Rv1, but not in PC3. Representative flow cytometry charts for (**A**-**C**) PNTA, (**D**-**F**) 22Rv1 and (**G**-**I**) PC3 cell populations. DHA induced apoptosis in 22Rv1 and PNT1A which was not clear for PC3. Two independent experiments were performed and acquired 2×10^4 events. Values were shown as mean of fold-change to vehicle incubation and SD. Representative cytograms were plotted in the first (vehicle) and second column (DHA) with mean of events in each gate. Legend: Annexin V-/7-AAD- – viable population; Annexin V-/7-AAD +—potentially necrosis; Annexin V + /7-AAD- – early apoptosis; Annexin V + /7-AAD + – late apoptosis. Legend: Ctrl – vehicle incubation; DHA – docosahexaenoic acid; evts – events

cells, the omega-3 rewired glucose metabolism towards oxidation in mitochondria and decreased their capacity to rely either on glycolysis or OXPHOS. Specifically, PNT1A and 22Rv1 had an increase in leucine levels upon DHA incubation, indicating that it is probably accumulated, supporting mitochondrial dysfunction. Interestingly, the metabolism of CRPC cells has been reported as avid for leucine which regulates cell proliferation [46, 47].

PNT1A is an immortalized epithelial prostate cell line that has been investigated as normal or non-malignant cell [48–50]. However, it has 10q arm deletion, chromosome losses, translocation involving chromosome 5, gene amplification and mRNA overexpression of *c-myc* and may occasionally form undifferentiated adenocarcinoma in nude mice [51]. This evidence supports that PNT1A as not normal (as PrEC cells), but not fully transformed either, being proposed as a model for PCa initiation [23,

27, 51]. In the present study, DHA showed the strongest effect on mitochondria in PNT1A cells. It showed a reduction in myo-inositol, a sugar reported to improve mitochondria function [52], detected in PCa samples [53] and suggested as an age-independent marker of PCa in human prostatic secretions [54]. We previously proposed mitochondria impairment in PNT1A cells by other methodology [27] and here, we described further the impact of DHA on it. In this cells, DHA led to increase in proton leak and had the most impaired spare capacity which occurs upon a shift from pyruvate oxidation in mitochondria to lactate [55]. Indeed, we observed higher basal ECAR in PNT1A, supporting our findings and suggesting a tentative to rescue homeostasis. In line with our work, DHA was reported to upregulate glycolysis-related genes concurrent to lactate production in benign tissue [56]. Therefore, it is likely that DHA seemed to induce PNT1A cells to reassume a glycolytic phenotype, usual of normal prostate cells, because of the mitochondrial dysfunction.

The increase in COX-1 to SDH-A ratio reflects an imbalance in mitochondria- and nuclei-encoded proteins, supporting the mitochondrial dysfunction, but also a deregulation of ETC components which are closely related with mitochondrial activity and morphology. The fission-like shape and network fragmentation observed here reflect organelle dysfunction [57], the glycolytic phenotype [58] and ROS overproduction. Fragmentation and dysfunction are also related with changes in the mitochondrial membrane composition. Indeed, increase in proton leak and impairment of the spare capacity are both tightly related with reduction in CL levels [59]. PG is a precursor of CL [60] which represents 15–20% of the inner mitochondrial membrane, stabilizes the ETC complexes [61] and is determinant on the cristae curvature due to its unique structure [62]. *n*-3 fatty acids enriched diet was reported to increase the unsaturation index of mitochondrial fatty acid in normal tissue [63]. The increase of 22:6 fatty acid composition indicates that DHA is incorporated into PG in all cell lines tested and hence likely into CL, turning the mitochondrial membrane itself more susceptible to oxidation by ROS [64]. This is particularly interesting for PNT1A due to the remarkable increase in PG unsaturation index. The increase of PUFAs in the membranes may cause lipoperoxidation and trigger cell death in PCa [65], mainly ferroptosis. Therefore, the increase in lipid droplets observed in our ultrastructural analysis, and also previously reported for PNT1A [27], may serve as an unsuccessful attempt to mitigate damages due to PUFAs oxidation [66, 67] which ultimately led to cell death.

In a different manner, for the tumor cells DHA impaired not only mitochondria but also glycolysis, a relevant outcome for CRPC. High glucose uptake correlates with a very-high risk for resistance to castration in PCa [68], stimulates cell proliferation and migration [69], and glycolysis acts as an anabolic pathway [70, 71]. Differently from PNT1A, it is likely that 22Rv1 and PC3 cells compensated the deficit from mitochondria dysfunction by routing glucose to OXPHOS. However, we did not found difference in the intracellular lactate levels, which needs further investigation, since other metabolites can affect its levels, such as amino acids. Specially in 22Rv1, DHA led to a decrease in basal ECAR indicating that anaerobic glycolysis was decreased while aerobic glucose increased at the expense of lipogenesis and likely of fatty acid β-oxidation, since o-acetylcarnitine levels decreased. Despite basal ECAR itself has been widely accepted as an indicator of glycolysis, determination of lactate levels in the medium and extracellular flux analysis with 2-deoxiglucose (2-DG) injection would strength our findings. Despite of this limitation, the decrease of *de novo* lipogenesis is a relevant outcome given that this is a hallmark in CRPC, being studied as a potential target [14, 15]. On the other hand, PC3 cells showed an increase either in aerobic glycolysis or lipogenesis from glucose carbons after DHA incubation. However, this did not mean a metabolic shift towards cell survival. In fact, the decrease in spare capacity along with glycolysis and glycolytic capacity features a metabolic weakness [55, 72]. Although apoptosis was not found at higher levels in tumor cells compared to PNT1A, the impairment of their spare capacity means that the potential for drug resistance is dramatically weakened. DHA was previously reported to sensitize cancer cells and increase the efficacy of chemotherapy [73–75], but the underlying mechanisms were not elucidated. Reduced maximum velocity indicates loss of ETC integrity [76] which is directly related with the spare capacity [77] that is associated with lipid oxidation [78]. In the present study, CRPC cells showed increased PG levels, which is harmful to mitochondria function [79] and suggests that CL synthesis is impaired. In addition, there was an increase in DHA-enriched PG, suggesting that these cells could be more susceptible to lipoperoxidation. However, CRPC cells seemed to balance the unsaturation in mitochondrial membrane by increasing saturated fatty acids. To the best of our knowledge, this is the first report of DHA incorporation in PG, the decrease of spare capacity in the CRPC cells and suggests that the omega-3 may be a potential co-adjuvant in chemotherapy.

The lower mitochondrial sensibility to DHA observed to PC3 is probably due its metabolic phenotype closer to glycolytic while AR-expressing cells like LNCaP are more oxidative [80]. This makes sense since LNCaP

has 4.6-fold more mitochondria mass compared with PrEC while PC3 has only 2.3-fold [28]. Such differences in mitochondrial physiology may explain the distinct response in the metabolic profile between the CRPC cells. 22Rv1, also an AR-expressing cell line, were more responsive to DHA than PC3 regarding the basal OCR, which can be supported by the decrease in aspartate levels since it can be derived mostly from oxaloacetate, an intermediate of TCA cycle. Despite not statistically significant ($p=0.03$, FDR = 0.1058), the increase in succinate levels in 22Rv1 may also indicate its accumulation which is related to mitochondria dysfunction [81, 82], including ROS generation [81]. Although less responsive, myo-inositol decreased in PC3 cells, indicating mitochondria damage, but also creatine phosphate increased, suggesting reduced breakdown and supporting the decrease in ATP production. Taken together, these findings show that among CRPC cells, 22Rv1 was more responsive to DHA than PC3. Indeed, DHA at same conditions led to G2/M arrest in PC3 [23]. These outcomes, in addition to our findings on cell death, may be also related with native characteristics of mitochondria in each cell line. PC3 cells show resistance in opening the permeability pore transition (mPTP) compared with other PCa cells, such as LNCaP [28], lower mitochondrial membrane hyperpolarization, an event related with ROS overproduction [23, 27], all crucial event for cell death. In addition, PC3 cells seemed to increase AMP levels ($p=0.02$, FDR = 0.11) which triggers AMPK and protects cells from cell death [83]. Taken together, this body of evidence indicates distinct resistance to cell death due to DHA, being non-malignant and CRPC androgen-positive cells more susceptible than androgen-negative cells. However, DHA led to important metabolic fragilities that may be combined with other therapies.

Conclusion

The summary of our findings was illustrated in Fig. 7. In conclusion, DHA induced the mitochondria dysfunction and lowered the capability of both non-malignant and CRPC cells to respond to insults. In addition, DHA helped to shift the glucose metabolism towards anaerobic glycolysis in non-malignant cells and to OXPHOS in CRPC, decreasing lipogenesis from glucose carbons

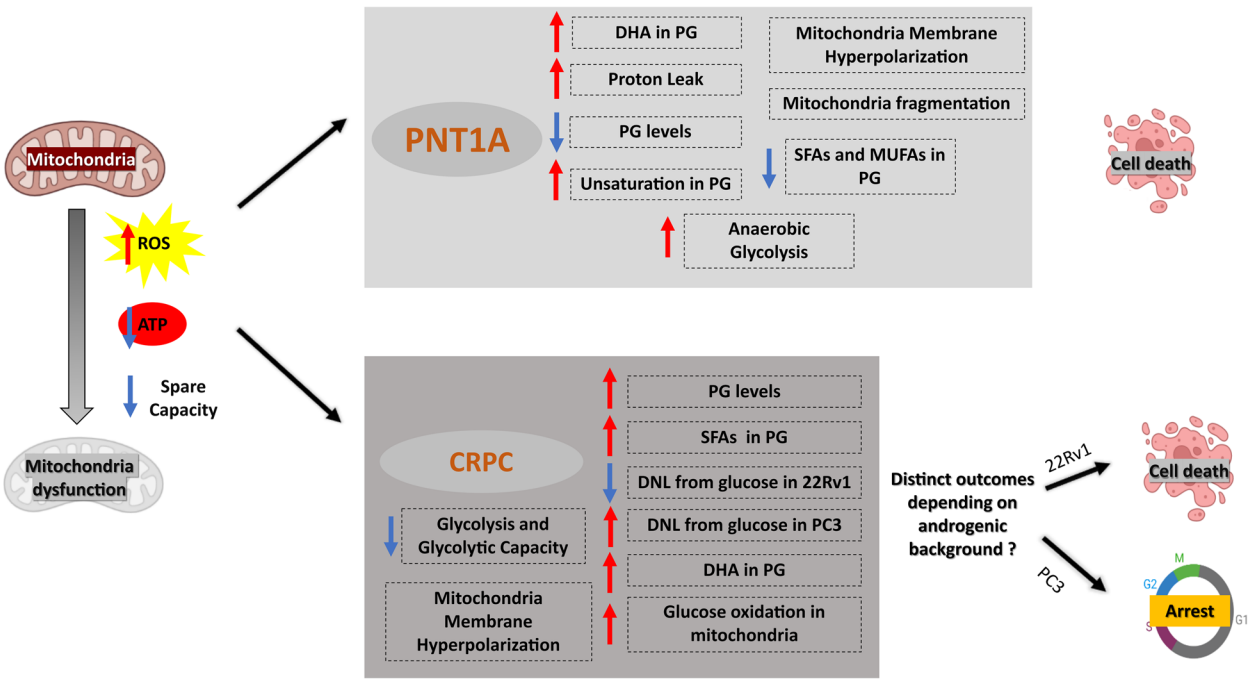

Fig. 7 Summary. DHA led to mitochondria dysfunction in non-malignant and CRPC cell lines by inducing ROS, impairment of ATP production and spare capacity. Such effect led to distinct outcomes depending on the molecular background. DHA turned PNT1A cells more glycolytic, increased proton leak and induced to changes in the mitochondrial membrane composition that raised the unsaturation status hence more susceptible to oxidative damage. Also, the omega-3 induced mitochondria fragmentation. In CRPC cells, DHA induced reprogramming of glucose metabolism, especially by decreasing glycolytic capacity, a crucial route for biosynthesis in proliferating cells, and shifting glucose towards its oxidation in mitochondria. In 22Rv1 it decreased *de novo* lipogenesis (DNL) while increased in PC3. However, the androgenic background seemed to determine the outcome of these alterations, being cell death triggered in PNT1A and 22Rv1 and cell cycle arrest in PC3. Legend: ROS – reactive oxygen species; ATP – adenosine triphosphate; CRPC – castrated-resistant prostate cancer; AR – androgen receptor; PG – phosphatidylglycerol; SFAs – saturated fatty acids; MUFAs – monounsaturated fatty acids; DHA – docosahexaenoic acid

mainly in 22Rv1. The omega-3 was incorporated in the mitochondrial membrane of all cell lines but increased the unsaturation index mostly in PNT1A. This cell line had the stronger effect due to DHA since it induced to mitochondrial fragmentation and triggered cell death. Therefore, DHA supplementation can be considered as a supplement to other therapeutic strategies that affect convergent pathways such as those outlined here, mainly in CRPC.

Abbreviations

^{1}H-NMR	Proton Nuclear Magnetic Resonance
7-AAD	7-Aminoactinomycin D
ALA	Alpha-Linoleic Acid
AMP	Adenosine Monophosphate
AR	Androgen Receptor
AR-V7	Androgen Receptor variant 7
ATCC	American Type Culture Collection
ATP	Adenosine Triphosphate
cDNA	Complementary DNA
CL	Cardiolipin
CO_2	Carbon Dioxide
COX-I	Cytochrome c Oxidase Subunit I
CRPC	Castration-Resistant Prostate Cancer
DHA	Docosahexaenoic Acid
DNA	Deoxyribonucleic Acid
DNL	De Novo Lipogenesis
DSS	3-(Trimethylsilyl)-1-propanesulfonic acid-d6 sodium salt
ECAR	Extracellular Acidification Rate
ELISA	Enzyme-Linked Immunosorbent Assay
EPA	Eicosapentaenoic Acid
ER	Endoplasmic Reticulum
ETC	Electron Transport Chain
FASN	Fatty Acid Synthase
FBS	Fetal Bovine Serum
FCCP	Carbonyl cyanide 4-(trifluoromethoxy)phenylhydrazone
FDA	Food and Drug Administration
FDR	False Discovery Rate
FID	Free Induction Decay
LC-ESI/MS/MS	Liquid Chromatography Electrospray Ionization Tandem Mass Spectrometry
LD	Lipid Droplet
LSI	Lipidomics Standards Initiative
mPTP	Mitochondrial Permeability Transition Pore
MRM	Multiple Reactions Monitoring
NAD +	Nicotinamide Adenine Dinucleotide
NIH	National Institutes of Health
NOESYPR1D	Nuclear Overhauser Effect Spectroscopy with Presaturation
OCR	Oxygen Consumption Rate
OLG	Oligomycin
O-PC	O-phosphocholine
OXPHOS	Oxidative Phosphorylation
PCA	Principal Component Analysis
PCa	Prostate cancer
PG	Phosphatidylglycerol
PUFAs	Polyunsaturated Fatty Acids
RFU	Relative Fluorescence Units
RLU	Relative Luminescence Units
RIPA buffer	Radio-Immunoprecipitation Assay buffer
RNA	Ribonucleic Acid
ROS	Reactive Oxygen Species
RPMI 1640	Roswell Park Memorial Institute 1640
RT	Room Temperature
RT-qPCR	Reverse Transcription Quantitative Polymerase Chain Reaction
SDH-A	Succinate Dehydrogenase A
SEM	Standard Error of the Mean
s*n*-3-GPC	Sn-3-Glycerophosphocholine
TCA	Tricarboxylic Acid
TEM	Transmission Electron Microscopy
TOCSY	Total Correlation Spectroscopy
TRAMP	Transgenic Adenocarcinoma of the Mouse Prostate
trypsin–EDTA	Trypsin-Ethylenediaminetetraacetic Acid
UDP-N-AcGlu	Uridine Diphosphate N-Acetylglucosamine
VIP	Variable Importance in Projection

Supplementary Information

The online version contains supplementary material available at https://doi.org/10.1186/s40170-024-00348-0.

Supplementary Material 1.

Acknowledgements
The authors are grateful to Dr. Hernandes Faustino Carvalho for cell culture infrastructure provided at University of Campinas (UNICAMP) and Sudha Rani Janaki Raman from Memorial Sloan Kettering Cancer Center (New York, USA) for assistance with extracellular flux analysis. We also thank the staff of the Life Sciences Core Facility (LaCTAD) at UNICAMP for the flow cytometry assays; the access to equipment and assistance provided by the National Institute of Science and Technology on Photonics Applied to Cell Biology (INFABIC-UNICAMP); and the Electron Microscopy Laboratory of the Brazilian Nanotechnology National Laboratory (LNNano) at Brazilian Center for Research in Energy and Materials (CNPEM; Campinas, São Paulo, Brazil) for technical support and assistance in image analysis.

Authors' contributions
G.H.T., R.M.G and M.L. contributed to the conception and design of the work. G.H.T., C.F.R., A.D.T.S., A.C., F.P.S., S.R.T. and I.P.C contributed to material preparation, data collection and analysis. All authors contributed to data interpretation. The first draft of the manuscript was written by G.H.T. with contributions of all authors. All authors read and approved the final manuscript.

Funding
Financial support was provided by São Paulo Research Foundation (FAPESP), Rio de Janeiro Research Foundation (FAPERJ), São José do Rio Preto Extension and Research Foundation (FAPERP), National Council for Scientific and Technological Development (CNPq) and Coordination for the Improvement of Higher Education Personnel (CAPES). The authors have received fellowships as follows: R.M.G. (2018/21891–4 FAPESP; 316398/2021–7 CNPq), G.H.T. (CAPES – Finance Code 001; FAPERP – 058/2018), F.P.S (FAPESP 2009/53989–4), I.P.C. (PROPe UNESP; 202.280/2018 FAPERJ) and A.D.T.S. (2019/15109–4 FAPESP; CAPES – Finance Code 001). This work was supported in part by National Cancer Institute grants: prostate cancer SPORE P50CA211024, P01 CA265768. We acknowledge support from the Prostate Cancer Foundation, the DoD W81XWH-19–1-0566, and the Pan Prostate Cancer Group (PPCG).

Availability of data and materials
The data used to support the findings of this study are available from the corresponding author upon request.

Declarations

Ethics approval and consent to participate
The data generated in this study did not require ethical approval. Consent to participate were not applicable.

Consent for publication
Not applicable.

Competing interests
The authors declare no competing interests.

Author details
[1]Institute of Biology, State University of Campinas, Campinas, São Paulo, Brazil. [2]Brazilian Biosciences National Laboratory (LNBio), Brazilian Center for Research in Energy and Materials (CNPEM), Campinas, São Paulo, Brazil.

[3]Department of Pathology and Laboratory Medicine, Weill Cornell Medicine, New York, NY, USA. [4]Department of Biological Sciences, IBILCE - UNESP. Rua Cristovão Colombo, 2265 Jardim Nazareth, São José Do Rio Preto, São Paulo 15054-000, Brazil. [5]Department of Biophysics, Institute of Biosciences, Humanities and Exact Science, São Paulo State University, São José Do Rio Preto, São Paulo, Brazil. [6]Institute of Medical Biochemistry and National Center for Structure Biology and Bioimaging (CENABIO), National Center for Nuclear Magnetic Resonance of Macromolecules, Federal University of Rio de Janeiro, Ilha Do Fundão, Rio de Janeiro, Brazil.

Received: 19 December 2023 Accepted: 29 June 2024
Published online: 07 August 2024

References

1. Siegel RL, Miller KD, Fuchs HE, Jemal A. Cancer statistics, 2022. CA Cancer J Clin. 2022;72:7–33.
2. Mansinho A, Macedo D, Fernandes I, Costa L. Castration-resistant prostate cancer: mechanisms, targets and treatment. Adv Exp Med Biol. 2018;1096:117–33.
3. Rawla P. Epidemiology of prostate cancer. World J Oncol. 2019;10:63–89.
4. Ryan CJ, Tindall DJ. Androgen receptor rediscovered: the new biology and targeting the androgen receptor therapeutically. J Clin Oncol. 2011;29:3651–8.
5. Vellky JE, Ricke WA. Development and prevalence of castration-resistant prostate cancer subtypes. Neoplasia. 2020;22:566–75.
6. Chandrasekar T, Yang JC, Gao AC, Evans CP. Mechanisms of resistance in castration-resistant prostate cancer (CRPC). Transl Androl Urol. 2015;4:365–80.
7. Sun L, Suo C, Li S-T, Zhang H, Gao P. Metabolic reprogramming for cancer cells and their microenvironment: beyond the Warburg effect. Biochim Biophys Acta Rev Cancer. 2018;1870:51–66.
8. Navarro C, Ortega Á, Santeliz R, Garrido B, Chacín M, Galban N, et al. Metabolic reprogramming in cancer cells: emerging molecular mechanisms and novel therapeutic approaches. Pharmaceutics. 2022;14(6):1303.
9. Costello LC, Franklin RB. A comprehensive review of the role of zinc in normal prostate function and metabolism; and its implications in prostate cancer. Arch Biochem Biophys. 2016;611:100–12.
10. Eidelman E, Twum-Ampofo J, Ansari J, Siddiqui MM. The metabolic phenotype of prostate cancer. Front Oncol. 2017;7:131.
11. Swinnen JV, Roskams T, Joniau S, Van Poppel H, Oyen R, Baert L, et al. Overexpression of fatty acid synthase is an early and common event in the development of prostate cancer. Int J Cancer. 2002;98:19–22.
12. Migita T, Ruiz S, Fornari A, Fiorentino M, Priolo C, Zadra G, et al. Fatty acid synthase: a metabolic enzyme and candidate oncogene in prostate cancer. J Natl Cancer Inst. 2009;101:519–32.
13. Zadra G, Photopoulos C, Loda M. The fat side of prostate cancer. Biochim Biophys Acta. 2013;1831:1518–32.
14. Zadra G, Ribeiro CF, Chetta P, Ho Y, Cacciatore S, Gao X, et al. Inhibition of de novo lipogenesis targets androgen receptor signaling in castration-resistant prostate cancer. Proc Natl Acad Sci USA. 2019;116:631–40.
15. Bastos DC, Ribeiro CF, Ahearn T, Nascimento J, Pakula H, Clohessy J, et al. Genetic ablation of FASN attenuates the invasive potential of prostate cancer driven by Pten loss. J Pathol. 2021;253:292–303.
16. Ribeiro CF, Rodrigues S, Bastos DC, Fanelli GN, Pakula H, Foiani M, et al. Blocking lipid synthesis induces DNA damage in prostate cancer and increases cell death caused by PARP inhibition. Sci Signal. 2024;17:eadh1922.
17. Butler LM, Perone Y, Dehairs J, Lupien LE, de Laat V, Talebi A, et al. Lipids and cancer: Emerging roles in pathogenesis, diagnosis and therapeutic intervention. Adv Drug Deliv Rev. 2020;159:245–93.
18. Escobar ELO, Gomes-Marcondes MCC, Carvalho HF. Dietary fatty acid quality affects AR and PPARgamma levels and prostate growth. Prostate. 2009;69:548–58.
19. Tamarindo GH, Gobbo MG, Taboga SR, Almeida EA, Góes RM. Melatonin ameliorates degenerative alterations caused by age in the rat prostate and mitigates high-fat diet damages. Cell Biol Int. 2021;45:92–106.
20. Labbé DP, Zadra G, Yang M, Reyes JM, Lin CY, Cacciatore S, et al. High-fat diet fuels prostate cancer progression by rewiring the metabolome and amplifying the MYC program. Nat Commun. 2019;10:4358.
21. Amaro GM, da Silva ADT, Tamarindo GH, Lamas C de A, Taboga SR, Cagnon VHA, et al. Differential effects of omega-3 PUFAS on tumor progression at early and advanced stages in TRAMP mice. Prostate. 2022;82(16):1491–504.
22. Shan K, Feng N, Cui J, Wang S, Qu H, Fu G, et al. Resolvin D1 and D2 inhibit tumour growth and inflammation via modulating macrophage polarization. J Cell Mol Med. 2020;24:8045–56.
23. Tamarindo GH, Góes RM. Docosahexaenoic acid differentially modulates the cell cycle and metabolism- related genes in tumor and pre-malignant prostate cells. Biochim Biophys Acta Mol Cell Biol Lipids. 2020;1865:158766.
24. Shin S, Jing K, Jeong S, Kim N, Song K-S, Heo J-Y, et al. The omega-3 polyunsaturated fatty acid DHA induces simultaneous apoptosis and autophagy via mitochondrial ROS-mediated Akt-mTOR signaling in prostate cancer cells expressing mutant p53. Biomed Res Int. 2013;2013:568671.
25. Xue M, Ge Y, Yu C, Zheng Z, He X, Zhao J. Apoptosis is induced by docosahexaenoic acid in breast cancer cells via death receptor and mitochondria-mediated pathways. Mol Med Report. 2017;16:978–82.
26. Abdi J, Garssen J, Faber J, Redegeld FA. Omega-3 fatty acids, EPA and DHA induce apoptosis and enhance drug sensitivity in multiple myeloma cells but not in normal peripheral mononuclear cells. J Nutr Biochem. 2014;25:1254–62.
27. Tamarindo GH, Ribeiro DL, Gobbo MG, Guerra LHA, Rahal P, Taboga SR, et al. Melatonin and docosahexaenoic acid decrease proliferation of PNT1A prostate benign cells via modulation of mitochondrial bioenergetics and ROS production. Oxid Med Cell Longev. 2019;2019:5080798.
28. Panov A, Orynbayeva Z. Bioenergetic and antiapoptotic properties of mitochondria from cultured human prostate cancer cell lines PC-3, DU145 and LNCaP. PLoS ONE. 2013;8:e72078.
29. Grupp K, Jedrzejewska K, Tsourlakis MC, Koop C, Wilczak W, Adam M, et al. High mitochondria content is associated with prostate cancer disease progression. Mol Cancer. 2013;12:145.
30. Mao P, Nakao K, Angrist A. Human prostatic carcinoma: an electron microscope study1. Cancer Res. 1996;26:955–73.
31. Burch TC, Rhim JS, Nyalwidhe JO. Mitochondria biogenesis and bioenergetics gene profiles in isogenic prostate cells with different malignant phenotypes. Biomed Res Int. 2016;2016:1785201.
32. Liu Y. Fatty acid oxidation is a dominant bioenergetic pathway in prostate cancer. Prostate Cancer Prostatic Dis. 2006;9:230–4.
33. Ahmad F, Cherukuri MK, Choyke PL. Metabolic reprogramming in prostate cancer. Br J Cancer. 2021;125:1185–96.
34. Caino MC, Altieri DC. Cancer cells exploit adaptive mitochondrial dynamics to increase tumor cell invasion. Cell Cycle. 2015;14:3242–7.
35. Scaglia N, Tyekucheva S, Zadra G, Photopoulos C, Loda M. De novo fatty acid synthesis at the mitotic exit is required to complete cellular division. Cell Cycle. 2014;13:859–68.
36. Bajpai P, Koc E, Sonpavde G, Singh R, Singh KK. Mitochondrial localization, import, and mitochondrial function of the androgen receptor. J Biol Chem. 2019;294:6621–34.
37. Lee YG, Nam Y, Shin KJ, Yoon S, Park WS, Joung JY, et al. Androgen-induced expression of DRP1 regulates mitochondrial metabolic reprogramming in prostate cancer. Cancer Lett. 2020;471:72–87.
38. Basu HS, Wilganowski N, Robertson S, Reuben JM, Cohen EN, Zurita A, et al. Prostate cancer cells survive anti-androgen and mitochondrial metabolic inhibitors by modulating glycolysis and mitochondrial metabolic activities. Prostate. 2021;81:799–811.
39. Eser PO, Vanden Heuvel JP, Araujo J, Thompson JT. Marine- and plant-derived ω-3 fatty acids differentially regulate prostate cancer cell proliferation. Mol Clin Oncol. 2013;1:444–52.
40. Rusca A, Di Stefano AFD, Doig MV, Scarsi C, Perucca E. Relative bioavailability and pharmacokinetics of two oral formulations of docosahexaenoic acid/eicosapentaenoic acid after multiple-dose administration in healthy volunteers. Eur J Clin Pharmacol. 2009;65:503–10.
41. Ghasemi Fard S, Wang F, Sinclair AJ, Elliott G, Turchini GM. How does high DHA fish oil affect health? A systematic review of evidence. Crit Rev Food Sci Nutr. 2019;59:1684–727.
42. Swanson D, Block R, Mousa SA. Omega-3 fatty acids EPA and DHA: health benefits throughout life. Adv Nutr. 2012;3:1–7.

43. Chong J, Xia J. Using metaboanalyst 4.0 for metabolomics data analysis, interpretation, and integration with other omics data. Methods Mol Biol. 2020;2104:337–60.
44. Bader DA, Hartig SM, Putluri V, Foley C, Hamilton MP, Smith EA, et al. Mitochondrial pyruvate import is a metabolic vulnerability in androgen receptor-driven prostate cancer. Nat Metab. 2019;1:70–85.
45. Dai W, Jiang L. Dysregulated mitochondrial dynamics and metabolism in obesity, diabetes, and cancer. Front Endocrinol (Lausanne). 2019;10:570.
46. Wang Q, Tiffen J, Bailey CG, Lehman ML, Ritchie W, Fazli L, et al. Targeting amino acid transport in metastatic castration-resistant prostate cancer: effects on cell cycle, cell growth, and tumor development. J Natl Cancer Inst. 2013;105:1463–73.
47. Tee AR. Metastatic castration-resistant prostate cancer hungers for leucine. J Natl Cancer Inst. 2013;105:1427–8.
48. Landim BC, de Jesus MM, Bosque BP, Zanon RG, da Silva CV, Góes RM, et al. Stimulating effect of palmitate and insulin on cell migration and proliferation in PNT1A and PC3 prostate cells: Counteracting role of metformin. Prostate. 2018;78:731–42.
49. Urbanek KA, Kowalska K, Habrowska-Górczyńska DE, Domińska K, Sakowicz A, Piastowska-Ciesielska AW. In vitro analysis of deoxynivalenol influence on steroidogenesis in prostate. Toxins (Basel). 2021;13(10):685.
50. Delafiori J, Faria AV de S, de Oliveira AN, Sales GM, Dias-Audibert FL, Catharino RR. Unraveling the metabolic alterations induced by Zika infection in prostate epithelial (PNT1a) and adenocarcinoma (PC-3) cell lines. J Proteome Res. 2023;22:193–203.
51. Degeorges A, Hoffschir F, Cussenot O, Gauville C, Le Duc A, Dutrillaux B, et al. Recurrent cytogenetic alterations of prostate carcinoma and amplification of c-myc or epidermal growth factor receptor in subclones of immortalized PNT1 human prostate epithelial cell line. Int J Cancer. 1995;62:724–31.
52. Condorelli RA, La Vignera S, Bellanca S, Vicari E, Calogero AE. Myoinositol: does it improve sperm mitochondrial function and sperm motility? Urology. 2012;79:1290–5.
53. Thomas MA, Nagarajan R, Huda A, Margolis D, Sarma MK, Sheng K, et al. Multidimensional MR spectroscopic imaging of prostate cancer in vivo. NMR Biomed. 2014;27:53–66.
54. Serkova NJ, Gamito EJ, Jones RH, O'Donnell C, Brown JL, Green S, et al. The metabolites citrate, myo-inositol, and spermine are potential age-independent markers of prostate cancer in human expressed prostatic secretions. Prostate. 2008;68:620–8.
55. Marchetti P, Fovez Q, Germain N, Khamari R, Kluza J. Mitochondrial spare respiratory capacity: mechanisms, regulation, and significance in non-transformed and cancer cells. FASEB J. 2020;34:13106–24.
56. Horn SS, Sonesson AK, Krasnov A, Moghadam H, Hillestad B, Meuwissen THE, et al. Individual differences in EPA and DHA content of Atlantic salmon are associated with gene expression of key metabolic processes. Sci Rep. 2019;9:3889.
57. Jheng H-F, Tsai P-J, Guo S-M, Kuo L-H, Chang C-S, Su I-J, et al. Mitochondrial fission contributes to mitochondrial dysfunction and insulin resistance in skeletal muscle. Mol Cell Biol. 2012;32:309–19.
58. Tomková V, Sandoval-Acuña C, Torrealba N, Truksa J. Mitochondrial fragmentation, elevated mitochondrial superoxide and respiratory supercomplexes disassembly is connected with the tamoxifen-resistant phenotype of breast cancer cells. Free Radic Biol Med. 2019;143:510–21.
59. Nguyen HM, Mejia EM, Chang W, Wang Y, Watson E, On N, et al. Reduction in cardiolipin decreases mitochondrial spare respiratory capacity and increases glucose transport into and across human brain cerebral microvascular endothelial cells. J Neurochem. 2016;139:68–80.
60. Chen WW, Chao YJ, Chang WH, Chan JF, Hsu YHH. Phosphatidylglycerol incorporates into cardiolipin to improve mitochondrial activity and inhibits inflammation. Sci Rep. 2018;8:4919.
61. Claypool SM, Oktay Y, Boontheung P, Loo JA, Koehler CM. Cardiolipin defines the interactome of the major ADP/ATP carrier protein of the mitochondrial inner membrane. J Cell Biol. 2008;182:937–50.
62. Ikon N, Ryan RO. Cardiolipin and mitochondrial cristae organization. Biochim Biophys Acta Biomembr. 2017;1859:1156–63.
63. Yu L, Fink BD, Herlein JA, Oltman CL, Lamping KG, Sivitz WI. Dietary fat, fatty acid saturation and mitochondrial bioenergetics. J Bioenerg Biomembr. 2014;46:33–44.
64. Watkins SM, Carter LC, German JB. Docosahexaenoic acid accumulates in cardiolipinand enhances HT-29 cell oxidant production. J Lipid Res. 1998;39:1583–8.
65. Tousignant KD, Rockstroh A, Poad BLJ, Talebi A, Young RSE, Taherian Fard A, et al. Therapy-induced lipid uptake and remodeling underpin ferroptosis hypersensitivity in prostate cancer. Cancer Metab. 2020;8:11.
66. Welte MA, Gould AP. Lipid droplet functions beyond energy storage. Biochim Biophys Acta Mol Cell Biol Lipids. 2017;1862 10 Pt B:1260–72.
67. Bailey AP, Koster G, Guillermier C, Hirst EMA, MacRae JI, Lechene CP, et al. Antioxidant role for lipid droplets in a stem cell niche of drosophila. Cell. 2015;163:340–53.
68. Lavallée E, Bergeron M, Buteau F-A, Blouin A-C, Duchesnay N, Dujardin T, et al. Increased prostate cancer glucose metabolism detected by 18F-fluorodeoxyglucose positron emission tomography/computed tomography in localised gleason 8–10 prostate cancers identifies very high-risk patients for early recurrence and resistance to castration. Eur Urol Focus. 2018;5(6):998–1006.
69. Rezende LP, Galheigo MRU, Landim BC, Cruz AR, Botelho FV, Zanon RG, et al. Effect of glucose and palmitate environment on proliferation and migration of PC3-prostate cancer cells. Cell Biol Int. 2019;43:373–83.
70. Vander Heiden MG, Cantley LC, Thompson CB. Understanding the Warburg effect: the metabolic requirements of cell proliferation. Science. 2009;324:1029–33.
71. Schiliro C, Firestein BL. Mechanisms of metabolic reprogramming in cancer cells supporting enhanced growth and proliferation. Cells. 2021;10(5):1056.
72. Lagadinou ED, Sach A, Callahan K, Rossi RM, Neering SJ, Minhajuddin M, et al. BCL-2 inhibition targets oxidative phosphorylation and selectively eradicates quiescent human leukemia stem cells. Cell Stem Cell. 2013;12:329–41.
73. Newell M, Brun M, Field CJ. Treatment with DHA modifies the response of MDA-MB-231 breast cancer cells and tumors from nu/nu mice to doxorubicin through apoptosis and cell cycle arrest. J Nutr. 2019;149:46–56.
74. Calviello G, Di Nicuolo F, Serini S, Piccioni E, Boninsegna A, Maggiano N, et al. Docosahexaenoic acid enhances the susceptibility of human colorectal cancer cells to 5-fluorouracil. Cancer Chemother Pharmacol. 2005;55:12–20.
75. Lim S-J, Lee E, Lee E-H, Kim S-Y, Cha JH, Choi H, et al. Docosahexaenoic acid sensitizes colon cancer cells to sulindac sulfide-induced apoptosis. Oncol Rep. 2012;27:2023–30.
76. Hill BG, Benavides GA, Lancaster JR, Ballinger S, Dell'Italia L, Jianhua Z, et al. Integration of cellular bioenergetics with mitochondrial quality control and autophagy. Biol Chem. 2012;393:1485–512.
77. Dranka BP, Hill BG, Darley-Usmar VM. Mitochondrial reserve capacity in endothelial cells: The impact of nitric oxide and reactive oxygen species. Free Radic Biol Med. 2010;48:905–14.
78. Hill BG, Dranka BP, Zou L, Chatham JC, Darley-Usmar VM. Importance of the bioenergetic reserve capacity in response to cardiomyocyte stress induced by 4-hydroxynonenal. Biochem J. 2009;424:99–107.
79. Pokorná L, Čermáková P, Horváth A, Baile MG, Claypool SM, Griač P, et al. Specific degradation of phosphatidylglycerol is necessary for proper mitochondrial morphology and function. Biochim Biophys Acta. 2016;1857:34–45.
80. Higgins LH, Withers HG, Garbens A, Love HD, Magnoni L, Hayward SW, et al. Hypoxia and the metabolic phenotype of prostate cancer cells. Biochim Biophys Acta. 2009;1787:1433–43.
81. Zhang Y, Zhang M, Zhu W, Yu J, Wang Q, Zhang J, et al. Succinate accumulation induces mitochondrial reactive oxygen species generation and promotes status epilepticus in the kainic acid rat model. Redox Biol. 2020;28:101365.
82. Lu Y-T, Li L-Z, Yang Y-L, Yin X, Liu Q, Zhang L, et al. Succinate induces aberrant mitochondrial fission in cardiomyocytes through GPR91 signaling. Cell Death Dis. 2018;9:672.
83. Barialai L, Strecker MI, Luger A-L, Jäger M, Bruns I, Sittig ACM, et al. AMPK activation protects astrocytes from hypoxia-induced cell death. Int J Mol Med. 2020;45:1385–96.

Publisher's Note